

# Optical Spectroscopy of nearby type1-LINERs

S. Cazzoli<sup>1</sup>, I. Márquez<sup>1</sup>, J. Masegosa<sup>1</sup>, A. del Olmo<sup>1</sup>, M. Pović<sup>2,1</sup>, O. González-Martín<sup>3</sup>, B. Balmaverde<sup>4</sup>, L. Hernández-García<sup>5</sup> and S. García-Burillo<sup>6</sup>

<sup>1</sup> IAA - Instituto de Astrofísica de Andalucía (CSIC), Apdo. 3004, 18080, Granada, Spain  
email: sara@iaa.es

<sup>2</sup> ESSTI/EORC - Ethiopian Space Science and Technology Institute, Entoto Observatory and Research Center, P.O. Box 33679, Addis Ababa, Ethiopia

<sup>3</sup> IRyA - Instituto de Radioastronomía y Astrofísica, 3-72 Xangari, 8701, Morelia, Mexico

<sup>4</sup> INAF - Osservatorio Astronomico di Brera, via Brera 28, I-20121 Milano, Italy

<sup>5</sup> Universidad de Valparaíso, Gran Bretana 1111, Playa Ancha, Valparaíso, Chile

<sup>6</sup> OAN - Observatorio Astronómico Nacional, Alfonso XII, 3, 28014, Madrid, Spain

**Abstract.** We present the highlights from our recent study of 22 local ( $z < 0.025$ ) type-1 LINERs from the Palomar Survey, on the basis of optical long-slit spectroscopic observations taken with TWIN/CAHA, ALFOSC/NOT and HST/STIS. Our goals were threefold: (a) explore the AGN-nature of these LINERs by studying the broad (BLR-originated)  $H\alpha\lambda 6563$  component; (b) derive a reliable interpretation for the multiple narrow components of emission lines by studying their kinematics and ionisation mechanism (via standard BPTs); (c) probe the neutral gas in the nuclei of these LINERs for the first time. Hence, kinematics and fluxes of a set of emission lines, from  $H\beta\lambda 4861$  to  $[SII]\lambda\lambda 6716, 6731$ , and the  $NaD\lambda\lambda 5890, 5896$  doublet in absorption have been modelled and measured, after the subtraction of the underlying light from the stellar component.

**Keywords.** galaxies: active, galaxies: kinematics and dynamics, techniques: spectroscopic.

## 1. Introduction

Low ionisation nuclear emission-line regions (LINERs) are a class of low-luminosity AGNs showing strong low-ionisation and faint high-ionisation emission lines (Heckman 1980). LINERs are interesting objects since they are the most numerous local AGN population bridging the gap between normal and active galaxies (Ho 2008).

Over the past 20 years, the ionising source in LINERs has been studied through a multi-wavelength approach via different tracers (Ho 2008). Nevertheless, a long standing issue is the origin and excitation mechanism of the ionised gas studied via optical emission lines. In addition to the AGN scenario, two more alternatives, such as pAGBs stars and shocks, have been proposed to explain the optical properties of LINERs (e.g. Singh et al. 2013). In LINERs, outflows are common as suggested by their  $H\alpha$  nuclear morphology (Masegosa et al. 2011). To open a new window to explore the AGN-nature and the excitation mechanism in LINERs, we propose to infer the role of outflows (identified as relatively broad component) in the broadening of emission lines. This broadening effect may limit the spectroscopic classification, as the contribution of outflows may overcome the determination of an eventually faint and broad  $H\alpha$  component from the BLR.

Ionised gas outflows are observed in starbursts and AGNs via long slit (e.g. Harrison et al. 2012) and integral field spectroscopy (e.g. Maiolino et al. 2017) of emission lines. The neutral gas in outflows have been studied in detail only in starbursts and luminous and ultra-luminous infrared galaxies (U/LIRGs) via the  $NaD$  absorption (e.g. Cazzoli et al. 2016).

In Cazzoli et al. 2018, hereafter C18, our goals were to investigate the AGN nature of type-1 LINERs and to characterize all the components by studying their kinematics and ionisation mechanisms. We also aimed to probe and study the neutral gas properties. For type-2 LINERs, see the contribution by L. Hermosa-Muñoz in this volume.

## 2. Sample, Data and Methods

The sample contains nearby ( $z < 0.025$ ) 22 type-1 LINERs (L1) selected from the Palomar Survey (see Ho et al. 1997). Spectroscopic data were gathered with the TWIN Spectrograph mounted on the 3.5m telescope of the Calar Alto Observatory (CAHA) and with ALFOSC attached to the 2.6m North Optical Telescope (NOT). We also analyzed archival spectra (red bandpass) for 12 LINERs (see Balmaverde et al. 2014 for details) obtained with the Space Telescope Imaging Spectrograph (STIS) on board the Hubble Space Telescope (*HST*). The data analysis is organised in three main steps:

### *Stellar Subtraction*

We applied the penalized PiXel fitting (pPXF; Cappellari 2017) and the STARLIGHT methods (Cid Fernandes et al. 2009) for modeling the stellar continuum. The stellar model is then subtracted to the observed to one obtain a interstellar medium spectrum.

### *Emission Lines*

The fit was performed simultaneously for emission lines from [OI] $\lambda\lambda$ 6300,6363 to [SII], with single or multiple Gaussian kinematic components (up two for forbidden lines and narrow  $H\alpha$ ). For the modeling of the  $H\alpha$ -[NII] $\lambda\lambda$ 6548,6584 blend, we tested three distinct models. Specifically, we considered either [SII] or [OI] (S- and O- models) or both ('mixed' M-model) as reference for tying central wavelengths and line widths (see example in Fig. 1). The latter model takes into account possible stratification density in the narrow line region. Then, a broad  $H\alpha$  component is added if needed to reduce significantly the residual. Finally, the best fitting (i.e. model, components, velocity shift and line widths) has been constraint to be the same for [OIII] $\lambda\lambda$ 4959,5007 and  $H\beta$  lines. Intensity ratios for [NII], [OI] and [OIII] lines were imposed following Osterbrock 2006.

### *Absorption Lines*

The NaD absorption doublet (8 detections) was modelled with one (i.e. two Gaussian profiles) or two components as in Cazzoli et al. 2014. The ratio of the equivalent widths of the two lines was allowed to vary from 1 to 2 (i.e. optically thick/thin limits, Spitzer 1978).

## 3. Main Results

NGC 4203 represents an extreme case as three line components are not sufficient to reproduce well the  $H\alpha$  profile, therefore, we excluded this L1 from the analysis.

For ground-based data, the S- and O- models reproduce well the line profiles in six of the cases each, while a larger fraction of cases (i.e. 9/21) require M-models for a satisfactory fit. Of the four possible combinations of the three components, as single narrow Gaussian per forbidden line is adequate in 6 out of 21 cases. A broad  $H\alpha$  component is required in the remaining four cases. In most cases (15/21), two Gaussians per forbidden line are required for a satisfactory modelling. Among these 15 cases, only in three cases a broad  $H\alpha$  component is required to reproduce well the observed profiles.

Velocities of the narrow components are close to rest frame varying within  $\pm 110 \text{ km s}^{-1}$ . The average velocity dispersion value for the narrow components is  $\sigma = 157 \text{ km s}^{-1}$ . For the second components the velocity range is large, from  $-350 \text{ km s}^{-1}$  to  $100 \text{ km s}^{-1}$ . The velocity dispersion varies between  $150$  and  $800 \text{ km s}^{-1}$  being generally broader (on average  $\sigma = 429 \text{ km s}^{-1}$ ) than for narrow components. A broad  $H\alpha$  component is required only in 7 out of the 21 LINERs, with FWHMs from  $1277 \text{ km s}^{-1}$  to  $3158 \text{ km s}^{-1}$ .

For none of the 11 *HST*/STIS spectra, the adopted best fit is obtained using the 0-model, finding a slightly large prevalence of best fits with M-models. In four cases, one Gaussian per forbidden line and narrow H $\alpha$  is adequate. In the remaining cases, two Gaussians are required for a good fit.

Narrow components have velocities between -100 and 200 km s $^{-1}$ ; the velocity dispersions vary between 120 and 270 km s $^{-1}$  (176 km s $^{-1}$ , on average). Similarly, the velocities of second component range from -200 to 150 km s $^{-1}$ . These second components are however broader, with velocity dispersion values between 300 and 750 km s $^{-1}$  (433 km s $^{-1}$ , on average). The broad component is ubiquitous. The FWHM of the broad H $\alpha$  components in *HST* spectra range from 2152 km s $^{-1}$  to 7359 km s $^{-1}$  (3270 km s $^{-1}$ , on average).

For the NaD absorption, in 7 out of 8 targets, a single kinematic component gives a good fit. Velocities of the neutral gas narrow components vary between -165 and 165 km s $^{-1}$ ; velocity dispersion values are in the range 104-335 km s $^{-1}$  (220 km s $^{-1}$ , on average).

## 4. Discussion

### Probing the BLR in L1

The analysis of Palomar spectra by Ho et al. (1997) indicated that all the LINERs in our selected sample show a broad H $\alpha$  component resulting in their classification as L1. Nevertheless, for ground-based data our detection rate for the broad component is only 33%, questioning the classification as L1 by Ho et al. (1997). For space-based data the broad component is ubiquitous in agreement with Balmaverde et al. 2014. By comparing our strategy and measurements with those by previous works (Sect. 5.1 in C18), we conclude that the detectability of the BLR-component is sensitive to the starlight decontamination and the choice of the template for the H $\alpha$ -[NII] blend. Moreover, a single Gaussian fit for the forbidden lines is an oversimplification in many cases.

### Kinematic classification of the components

The distribution of the velocity for narrow and second components as a function of their velocity dispersion is presented in Fig. 2. We identified four areas corresponding to different kinematical explanations: rotation, candidate for non-rotational motions and non-rotational-motions (with broad blue/redshifted lines produced by outflows/inflows). For both ground- and space-based data, the kinematics of the narrow component can be explained with rotation in all cases (Fig. 2 left) whereas that of the second components encompass all possibilities (Fig. 2, right). From our ground-based data, we identified 6 out of 15 (40%) cases that may be interpreted as outflows. Outflow-components have velocities varying from -15 km s $^{-1}$  to -340 km s $^{-1}$ , and velocity dispersions in the range of 450-770 km s $^{-1}$  (on average, 575 km s $^{-1}$ ). We did not interpret as outflows any case in *HST*/STIS data. These results partially disagree with studies of the H $\alpha$  morphology in LINERs which indicate that outflows are frequent in LINERs. A possible explanation is that the extended nature of outflows is not fully captured by the *HST*/STIS spectra.

### Ionisation mechanisms from standard ‘BPT (Baldwin, Phillips & Terlevich)-diagrams’

The line ratios for the narrow component are generally consistent with those observed in AGNs (either Seyfert or LINERs), excluding the star-formation or pAGBs as the dominant ionization mechanism (see Fig. 9 in C18). For the second component, we reproduced the observed line ratios with the shock-models by Groves et al. 2004. We combined the data points and models for the [O I]/H $\alpha$  BPT diagram (Baldwin et al. 1981), the most reliable for studying shocks (Allen et al. 2008) shown in Fig. 3, with the kinematical classification shown in Fig. 2. Models at low velocities (< 300 km s $^{-1}$ ) indicate the presence of mild-shocks associated to perturbations of rotation (Fig. 3 center). At higher velocities (> 400 km s $^{-1}$ ) shocks are produced by non-rotational motions (Fig. 3 right).

### A lack of neutral outflows?

According to the adopted kinematic classification all the neutral gas kinematic components (except one) could be interpreted as rotation. The possible explanation of the lack of neutral gas non-rotational motions, such as outflows, is twofold. First, the neutral component in outflows is possibly less significant in AGNs than in starbursts galaxies and U/LIRGs. Secondly, such a null detection rate might be a consequence of the conservative limits we assumed, as ionised and neutral gas correspond to different phases of the outflows, and hence these may have a different kinematics (e.g. Cazzoli et al. 2016).

## 5. Conclusions

- The AGN nature of L1. The detection of the BLR-component is sensitive to the starlight subtraction, the template for the H $\alpha$ -[NII] blend and the assumption of a single Gaussian fit (often an oversimplification); NLR stratification might be often present in L1.
- Kinematics of emission lines and their classification. The kinematics of the narrow component can be explained with rotation in all cases whereas that of the second components encompass all possibilities. From our ground-based data, the detection rate of outflows is 40%. We did not interpret as outflows any case in *HST*/STIS data.
- Ionisation mechanisms. Our results favor the AGN photoionisation as the dominant mechanism of ionisation for the narrow component. Shocks models (at the observed velocities) are able to reproduce the observed line ratios of the second component.
- Neutral gas in L1. The neutral gas is found to be in rotation. Neutral gas outflows are possibly less significant in AGNs or the limits we assumed are too conservative.

## Acknowledgements

We thank the financial support by the Spanish MCIU and MEC, grants SEV-2017-0709 and AYA 2016-76682-C3. SC thanks the IAU for the travel grant.

## References

- Allen M. G., Groves B. A., Dopita M. A. et al. 2008, *ApJS*, 178, 20  
 Balmaverde & Capetti 2014, *A&A*, 563, A119  
 Baldwin, Phillips & Terlevich 1981, *PASP*, 93, 5  
 Binette L., Magris C. G., Stasinska G., Bruzual A. G 1994, *A&A*, 292, 13  
 Cazzoli S., Marquez I., Masegosa J. et al. 2018, *MNRAS*, 480, 1106  
 Cazzoli S., Arribas S., Maiolino R. & Colina L. 2016, *A&A*, 590, A125  
 Cazzoli S., Arribas S., Colina L., et al. 2014, *A&A*, 569, A14  
 Cappellari M. 2017, *MNRAS*, 466, 798  
 Cid Fernandes R., Stasinska G., Schlickmann M. et al. 2009, *Rev. Mex. Astron. Astrofis.*, 35, 127  
 Filippenko A. V. & Terlevich R. 1992, *ApJ*, 397, L79  
 Groves B. A., Dopita M. A. & Sutherland R. S. 2004, *ApJS*, 153, 75  
 Heckman 1980, *A&A*, 87, 152  
 Ho L. C., Filippenko A. V., Sargent W. L. W. 1997, *ApJS*, 112, 315  
 Ho L. C. 2008, *ARA&A*, 46, 475  
 Kewley L. J., Groves B., Kauffmann G. & Heckman T. 2006, *MNRAS*, 372, 961  
 Kauffmann G., Heckman, T., Tremonti, C. et al. 2003, *MNRAS*, 346, 1055  
 Maiolino R., Russel H., Fabian A. et al. 2017, *Nature*, 544, 202  
 Masegosa J., Marquez I., Ramirez A. et al. 2011, *A&A*, 527, A23  
 Osterbrock D. E., et al. 2006, *Astrophysics of Gaseous Nebulae and Active Galactic Nuclei*  
 R. Singh G., van de Ven K., Jahnke, M. et al. 2013, *A&A*, 558, A43  
 Spitzer L. 1978, *Physical Processes in the Interstellar Medium*. Wiley-Interscience, New York

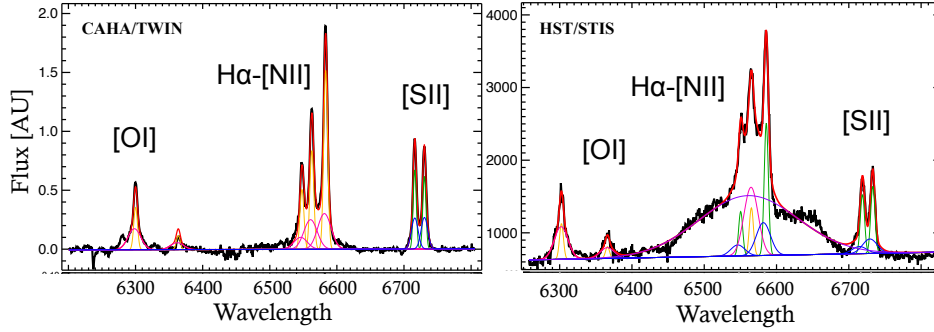


**Figure 1.** Gaussian fit to the ground- (left) and space- (right) based spectra for NGC4450 in the  $H\alpha$  region. We marked with different colours the components required to model the emission lines. The red curve shows the total contribution from the fit.

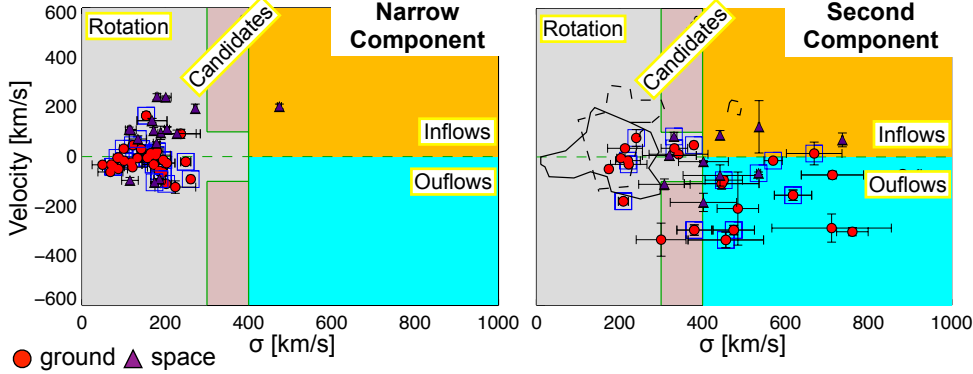


**Figure 2.** Observed velocity dispersion-velocity plane for narrow (left) and second (right) components. Red circles and purple triangles mark the measurements from ground- and space-based data, respectively. An additional blue box marks those LINERs for which the fitting of the  $H\alpha$  profile is less reliable (see C18). In the right panel, we report the measurements of the narrow component with contours (continuous and dashed lines are for ground- and space-based data, respectively). The coloured areas indicate different classifications (labelled on the panels).

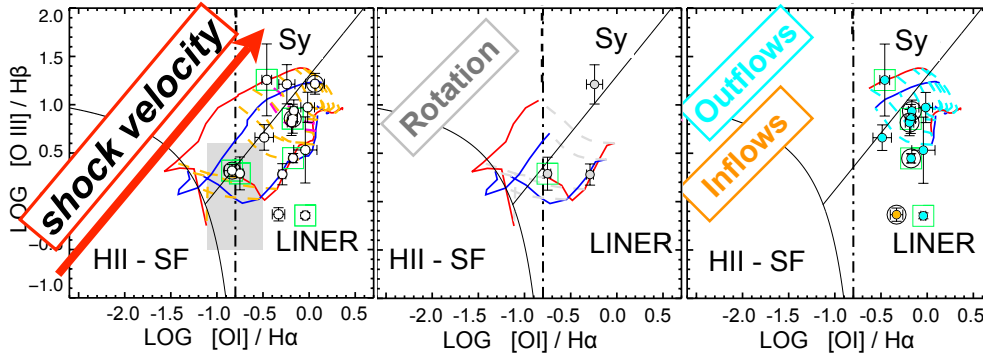


**Figure 3.** *Left:* optical standard [OI] BPT diagram (Baldwin et al. 1981) for the second component obtained from our ground-based spectroscopy (circles). In all the panels an additional circle marks those LINERs for which a broad component is required to reproduce the  $H\alpha$  profile. Light-green square are as in Fig. 2. Black lines represent the dividing curves between HII regions, Seyferts, and LINERs from Kewley et al. 2006 and Kauffmann et al. 2003, and weak-[OI] and strong-[OI] LINERs from Filippenko & Terlevich 1992. Gray boxes show the predictions of photoionisation models by pAGB stars by Binette et al 1994. The predictions of shock+precursor-ionisation models from Groves et al. 2004 with  $n_{e1} = 100 \text{ cm}^{-3}$  (blue) and  $n_{e1} = 1000 \text{ cm}^{-3}$  (red) are overlaid. Iso-velocities are marked with yellow dashed-lines. *Center and Right panels* are the same but considering different shock-velocities (colour coded according to Fig. 2).